JOURNAL OF GEOSPACE SCIENCE

Vol. 6 No. 2 (2026)

E-ISSN : 2413-6093
https://jogss.org

Transient Pore-Pressure Imaging of Plug Formation during Caisson Penetration

Matheus Almeida

Department of Materials Engineering, Faculty of Engineering, Universidade do Estado do Rio de Janeiro, Rio de Janeiro, Brazil

ABSTRACT

The installation of open-ended caisson foundations for offshore structures is frequently complicated by the phenomenon of soil plugging, which significantly alters penetration resistance and foundation stability. Understanding the real-time dynamics of plug formation remains a critical challenge in geotechnical engineering due to the opaque nature of soil-structure interactions and the limitations of traditional post-installation measurements. This paper presents a novel approach to monitoring and analyzing soil plugging through transient pore-pressure imaging during caisson penetration. By deploying a high-density array of miniature piezoresistive sensors within a large-scale calibration chamber, we successfully captured the spatiotemporal evolution of excess pore-water pressures both inside and outside the caisson. The data was processed using advanced interpolation algorithms to generate dynamic, two-dimensional cross-sectional images of pore-pressure fields. These images reveal the localized shear zones, the transition from fully coring to partially plugged states, and the eventual formation of a rigid soil plug. Our findings demonstrate that abrupt changes in inner pore-pressure gradients serve as highly reliable precursors to plug locking. The continuous imaging technique offers unprecedented insights into the hydromechanical coupling that governs plug friction and arching effects. The results provide a robust empirical basis for refining predictive models of penetration resistance, ultimately contributing to safer and more cost-effective offshore foundation design.

KEYWORDS

Soil Plugging, Caisson Foundations, Pore-Pressure Imaging, Offshore Geotechnics, Penetration Resistance.. ..

1. Introduction

1.1 Background on Caisson Foundations

The rapid expansion of offshore renewable energy and deep-water oil and gas exploration has necessitated the development of robust, cost-effective, and highly reliable foundation systems. Among these, open-ended steel pipe piles and suction caissons have emerged as the preferred solutions for anchoring large

offshore structures, including wind turbine generators, tension leg platforms, and floating production storage and offloading units. The preference for open-ended caissons stems from their ability to be installed in deep waters with significantly lower driving energy compared to closed-ended piles, minimizing the environmental impact of underwater noise and reducing the structural fatigue on the pile material during installation. As the caisson is driven, jacked, or suctioned into the seabed, the soil enters the hollow interior, ideally allowing the structure to penetrate with minimal end-bearing resistance. This fundamental installation advantage has made open-ended caissons ubiquitous in modern marine geotechnics. However, the interaction between the penetrating caisson and the surrounding saturated seabed soil is extraordinarily complex, governed by dynamic hydromechanical processes that dictate the ultimate bearing capacity and the feasibility of reaching the target penetration depth [1]. The continuous entry of soil into the caisson interior is rarely a passive process; it involves intense localized shearing, volumetric dilation or contraction, and massive fluctuations in pore-water pressure. As the industry moves toward larger diameter caissons and deeper water installations, the empirical methods traditionally used to predict installation behavior are increasingly falling short, highlighting a pressing need for advanced diagnostic techniques and a deeper fundamental understanding of the soil-structure interaction during the installation phase. The installation process in saturated soils is fundamentally a large-strain, moving-boundary problem characterized by severe soil remolding and the generation of significant excess pore-water pressures [2]. When the caisson penetrates the soil, the finite thickness of the caisson wall displaces an equivalent volume of soil, forcing it either outward into the surrounding soil mass or inward into the caisson cavity. The trajectory of this displaced soil and the distribution of the resulting stresses are highly dependent on the permeability of the soil, the rate of penetration, and the boundary conditions established by the caisson geometry. In highly permeable soils such as clean sands, the generated pore pressures may dissipate almost instantaneously, leading to drained penetration behavior where effective stresses and frictional resistance dominate. Conversely, in low-permeability soils such as soft marine clays, the penetration occurs under undrained conditions, resulting in massive accumulations of excess pore pressure that temporarily reduce effective stresses and alter the shearing resistance of the soil. The transitional regimes, often encountered in silty sands or stratified seabed profiles, exhibit partial drainage, making the prediction of penetration resistance exceptionally difficult. Traditional geotechnical investigations rely heavily on pre-installation site characterizations and post-installation load tests, providing only static snapshots of the foundation capacity. While these conventional methods are well-established, they offer virtually no real-time data on the dynamic evolution of the soil state during the actual penetration process, leaving engineers blind to the transient mechanisms that ultimately dictate the success or failure of the installation.

1.2 The Phenomenon of Plug Formation

A critical phenomenon that dramatically alters the installation mechanics of open-ended caissons is the formation of a soil plug within the inner cavity. During the initial stages of penetration, the soil typically flows freely into the caisson, a condition referred to as the fully coring mode. In this state, the inner soil column advances at the same rate as the external soil surface, and the penetration resistance is primarily composed of the external shaft friction and the annular end-bearing capacity of the caisson wall. However, as penetration progresses, the frictional resistance acting on the inner wall of the caisson steadily increases due to the growing contact area and the accumulation of lateral earth pressures [3]. Simultaneously, the internal soil column undergoes complex radial compression and vertical arching. Arching occurs when the shear stresses along the inner wall transfer the vertical loads to the center of the soil column, creating a self-supporting dome-like structure that effectively resists further soil intrusion. When the internal friction and arching forces exceed the end-bearing capacity of the underlying soil, the soil column locks against the caisson wall, transitioning the system into a partially plugged or fully plugged state. In a fully plugged condition, the caisson behaves as if it were closed-ended, causing a sudden and dramatic spike in penetration resistance that can easily exceed the capacity of the installation equipment, leading to premature refusal. Understanding and predicting this transition from coring to plugging is one of the most

significant challenges in offshore foundation design.

The mechanics of plug formation are intrinsically linked to the transient pore-pressure dynamics within the soil mass. In saturated porous media, the rapid application of stress during penetration induces excess pore pressures that initially carry the applied load. As these pressures dissipate, the load is transferred to the soil skeleton, increasing the effective stress and the corresponding frictional resistance. Inside the confined geometry of the caisson cavity, the drainage paths are highly restricted, leading to complex spatial and temporal distributions of pore pressure. Conventional theoretical models of soil plugging have largely relied on effective stress frameworks that assume static or steady-state conditions, often ignoring the highly transient nature of pore-pressure generation and dissipation during continuous penetration [4]. Consequently, these models frequently fail to capture the sudden onset of plugging, particularly in layered soils or under variable penetration rates. To overcome these limitations, there is a critical need for advanced experimental techniques capable of visualizing the internal state of the soil in real-time. By mapping the transient pore-pressure fields, researchers can directly observe the hydromechanical precursors to plug locking, such as localized pressure gradients that indicate shear band formation or the sudden drop in inner pore pressure that signals the initiation of soil arching. This paper aims to bridge this knowledge gap by introducing a comprehensive pore-pressure imaging methodology, offering a high-resolution window into the dynamic processes that govern plug formation during caisson penetration.

2. Literature Review and Theoretical Framework

2.1 Previous Studies on Soil Plugging

The study of soil plugging in open-ended tubular piles and caissons has a rich history in geotechnical engineering, driven primarily by the needs of the offshore oil and gas sector. Early empirical studies focused on correlating the final plug length with the overall pile geometry, the installation method, and the initial soil density. Researchers established various metrics to quantify plugging, most notably the Plug Length Ratio, defined as the final length of the soil plug divided by the total penetration depth, and the Incremental Filling Ratio, which measures the rate of plug growth relative to the incremental penetration of the pile. Extensive field data and centrifuge tests demonstrated that the Incremental Filling Ratio typically begins near unity in the fully coring phase and progressively approaches zero as the pile becomes fully plugged. Based on these observations, several semi-empirical design methods were developed, such as those incorporated into the American Petroleum Institute recommended practices [5]. These methods typically assume that plugging occurs when the cumulative internal shaft friction equals the bearing capacity of the soil beneath the plug toe. While these static force-equilibrium approaches provide a practical framework for estimating ultimate bearing capacity, they are inherently limited by their inability to account for the dynamic, highly non-linear processes that occur during the actual penetration event.

Advancements in computational modeling, particularly in the realm of finite element and discrete element methods, have provided deeper theoretical insights into the micromechanics of soil plugging. Large-deformation finite element analyses utilizing Arbitrary Lagrangian-Eulerian formulations or Coupled Eulerian-Lagrangian techniques have successfully simulated the gross physical displacement of the soil during pile driving and jacking. These numerical studies highlighted the severe stress concentrations around the pile tip and the formation of distinct shear bands that dictate the flow of soil into the plug. Discrete element modeling, which treats the soil as a collection of individual interacting particles, has been particularly useful in elucidating the phenomenon of soil arching. Researchers employing discrete element models observed that as the internal shaft friction increases, strong force chains develop across the diameter of the plug, transferring vertical stresses to the pile walls and effectively shielding the lower portion of the plug from further densification [6]. Despite these computational successes, numerical models require rigorous calibration and validation against high-quality experimental data. Most physical modeling efforts have been constrained by the difficulty of installing sensors within the advancing plug without disturbing the very processes they are meant to measure. Consequently, validation has largely relied on post-test measurements of plug length and gross resistance, leaving the transient internal mechanics largely inferred rather than directly observed.

2.2 Transient Pore-Pressure Dynamics

The generation and dissipation of transient pore-water pressure is a fundamental governing mechanism in the penetration of objects into saturated soils. According to classical critical state soil mechanics, when a saturated soil is subjected to rapid undrained shearing, it will either generate positive excess pore pressure if it is contractive, or negative excess pore pressure if it is dilative [7]. During caisson penetration, the massive displacement of soil by the advancing wall induces extreme shear strains and high mean total stresses. In contractive loose soils, this results in significant positive excess pore pressures that drastically reduce the effective stress and the corresponding shear strength, facilitating easier penetration. In dense, heavily overconsolidated soils, the tendency to dilate can cause localized negative pore pressures, leading to an increase in effective stress and a phenomenon known as set-up, where penetration resistance increases dramatically [8]. The rate at which these transient pressures dissipate is governed by the hydraulic conductivity of the soil and the length of the drainage paths, as described by classical consolidation theory. However, the geometric confinement of the caisson cavity fundamentally alters these drainage boundary conditions. Soil trapped within the plug is radially constrained by the impermeable steel walls, forcing all fluid flow to occur vertically. This one-dimensional drainage condition significantly retards pore pressure dissipation, prolonging the undrained state and delaying the mobilization of internal shaft friction. Recent experimental efforts have attempted to measure these pore pressure effects using instrumented pile probes equipped with localized piezocones or flush-mounted transducers. These studies confirmed that excess pore pressures are highly concentrated near the pile tip and decay exponentially with vertical distance along the pile shaft. However, point measurements provide only a limited understanding of the complex spatial gradients that drive fluid flow and effective stress transfer within the soil mass. The lack of continuous, full-field data has hindered the development of accurate predictive models for plug formation. To fully understand the mechanisms of plugging, it is necessary to capture the complete spatiotemporal distribution of pore pressures throughout the entire penetration event. This requires a paradigm shift from discrete point monitoring to continuous spatial imaging. By reconstructing the dynamic pore pressure field, it becomes possible to directly visualize the hydraulic gradients, identify regions of localized dilation or contraction, and pinpoint the exact moment and location where soil arching initiates [9]. The theoretical framework for interpreting such data lies in coupling the transient hydraulic gradients with the evolving effective stress state, thereby linking the physical observation of the pressure field to the mechanical reality of plug locking and resistance mobilization.

3. Methodology and Analytical Model

3.1 Experimental Design and Sensor Setup

To achieve the objective of continuous pore-pressure imaging during caisson penetration, a state-of-the-art physical modeling program was developed utilizing a large-scale geotechnical calibration chamber. The cylindrical chamber, constructed from thick-walled stainless steel, possesses an internal diameter of 1.5 meters and a height of 2.0 meters, providing sufficient volume to minimize boundary interference during the penetration of the scaled caisson model. The test soil utilized was a highly uniform quartz sand, selected for its well-characterized critical state properties and predictable hydraulic conductivity. The sand was deposited into the chamber using an automated fluidization and pluviation system, which precisely controlled the drop height and deposition rate to achieve a highly homogenous, fully saturated soil bed with a consistent relative density. De-aired water was continuously circulated through the base of the chamber during the preparation phase to ensure a baseline saturation level exceeding 99 percent, a critical requirement for accurate pore-pressure measurements. The initial state parameters and fundamental physical properties of the prepared soil bed are detailed in Table 1 below.

Table 1: Soil Properties and Initial State Parameters

Parameter	Symbol	Value	Unit
Specific Gravity	G_s	2.65	Dimensionless

Mean Grain Size	D_50	0.22	Millimeters
Minimum Void Ratio	e_min	0.58	Dimensionless
Maximum Void Ratio	e_max	0.89	Dimensionless
Initial Relative Density	D_r	65.0	Percent
Hydraulic Conductivity	k_v	1.4e-4	Meters per second

The scaled open-ended caisson model was fabricated from high-strength aluminum alloy to minimize weight while ensuring structural rigidity. The model possessed an outer diameter of 150 millimeters, a wall thickness of 5 millimeters, and a total length of 1000 millimeters. To capture the transient pore-pressure fields, a high-density array of ultra-miniature piezoresistive pressure transducers was strategically deployed. Instead of placing sensors exclusively on the caisson itself, which only measures boundary pressures, a network of 48 independent sensors was embedded directly within the soil mass at predetermined spatial coordinates. These sensors were suspended using micro-gauge tension wires that provided negligible resistance to soil movement, ensuring that the structural presence of the sensors did not artificially induce localized arching or disrupt the natural formation of the plug [10]. Additionally, a secondary array of 12 flush-mounted transducers was integrated into the inner and outer walls of the caisson model. All sensors were connected to a high-speed synchronous data acquisition system capable of sampling at a rate of 1000 Hertz, providing exceptional temporal resolution. The penetration force was applied using a servo-hydraulic actuator, programmed to advance the caisson at a constant, highly controlled rate of 20 millimeters per second. The detailed calibration metrics of the sensor arrays are summarized in Table 2.

Table 2Sensor Array Calibration Metrics

Sensor Type	**Placement Location**	**Measurement Range**	**Accuracy Tolerance**
Embedded Miniature	Soil Mass Matrix	0 to 500 Kilopascals	0.25 Percent
Flush-Mounted Wall	Caisson Inner Wall	0 to 1000 Kilopascals	0.15 Percent
Load Cell Unit	Actuator Head	0 to 50 Kilonewtons	0.10 Percent
Laser Displacement	Top of Soil Plug	0 to 1000 Millimeters	0.05 Percent

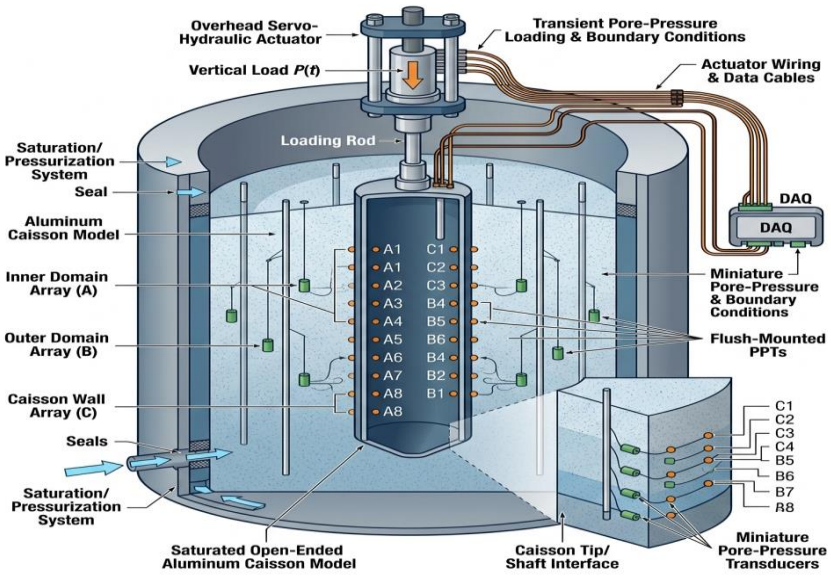


Figure 1Comprehensive Schematic of Experimental Calibration Chamber and Sensor Array Deployment for Transient Pore

The execution of each test followed a rigorous, standardized protocol to ensure repeatability and data integrity. Following the saturation and consolidation phase, the baseline hydrostatic pore pressures were recorded to establish a zero reference. The servo-hydraulic actuator was then engaged, driving the caisson smoothly into the soil bed. Throughout the penetration event, an independent laser displacement sensor, positioned above the chamber and aimed down the interior of the caisson, continuously measured the elevation of the internal soil plug. The differential between the caisson penetration depth and the internal soil elevation provided a real-time, highly accurate measurement of the plug length. The data acquisition system simultaneously logged the applied load, caisson displacement, plug elevation, and the massive stream of analog voltage signals from the 60 independent pore-pressure transducers [11]. Post-test procedures involved carefully excavating the chamber to verify the final plug length and to inspect the embedded sensor array for any positional shifting, ensuring the spatial coordinates used in the subsequent imaging reconstruction algorithms remained valid.

3.2 Formulation of the Pore-Pressure Model

Transforming the massive dataset of discrete, time-series pressure readings into continuous spatial images required the development of a robust analytical model and advanced data interpolation algorithms. The raw voltage signals from the transducers were first subjected to a low-pass digital filter to eliminate high-frequency electrical noise and vibration artifacts induced by the servo-hydraulic actuator. The filtered data was then converted into engineering units representing excess pore-water pressure, defined as the total measured pressure minus the initial hydrostatic baseline. To generate the spatiotemporal images, a dynamic spatial interpolation technique based on ordinary kriging was implemented. Kriging is a geostatistical method that estimates values at unknown locations based on a weighted average of surrounding known data points, with the weights determined by a spatial covariance function. A custom semivariogram model was optimized for the specific cylindrical geometry and anticipated anisotropic pressure gradients of the caisson penetration problem. Because the caisson was continuously moving, the spatial coordinates of the wall-mounted sensors relative to the static soil sensors were constantly updating. The interpolation algorithm incorporated this moving boundary condition by recalculating the spatial matrix at discrete depth intervals of 5 millimeters, resulting in a continuous sequence of two-dimensional axisymmetric cross-sectional images that mapped the entire internal and external fluid pressure fields.

The theoretical interpretation of these images relies on the fundamental mechanics of transient fluid flow and effective stress coupling in porous media. The dissipation of excess pore-water pressure within the soil plug is mathematically described by the three-dimensional transient diffusion equation. By applying

the principles of conservation of mass and Darcy's law for fluid flow through an isotropic porous medium, the governing equation for pore pressure evolution can be rigorously formulated. The spatial and temporal variation of the excess pore pressure is driven by the volumetric strains induced by the penetrating structure and regulated by the coefficient of consolidation. This fundamental relationship is expressed in the following block mathematical formula:

$$\frac{\partial u}{\partial t} = C_v\left(\frac{\partial^2 u}{\partial r^2} + \frac{1}{r}\frac{\partial u}{\partial r} + \frac{\partial^2 u}{\partial z^2}\right) + \alpha\frac{\partial \sigma_v}{\partial t}$$

In this standard mathematical formulation, the term on the left represents the rate of change of excess pore-water pressure with respect to time. On the right side, the parameter represents the three-dimensional coefficient of consolidation, which is a function of the soil permeability and volumetric compressibility [12]. The terms within the parentheses represent the Laplacian operator in cylindrical coordinates, accounting for radial and vertical pressure gradients. The final term represents the source function, where the scalar multiplier relates the generation of pore pressure to the rate of change of total vertical stress imposed by the advancing caisson tip. This equation clearly demonstrates how steep pressure gradients in the radial direction can drive fluid outward, while vertical gradients dictate flow up through the soil plug. To quantify the state of the soil plug, the macroscopic phenomenological observation of plug length must be mathematically correlated to the internal effective stress state. The continuous logging of plug length permits the calculation of the Incremental Filling Ratio, which serves as the primary physical indicator of plugging status. The dynamic resistance offered by the soil plug is a direct function of the depth-dependent effective radial stress acting on the inner wall and the corresponding interface friction angle. As the excess pore pressures generated at the tip propagate upward and gradually dissipate, the effective stress recovers, increasing the frictional resistance. The total internal resisting force accumulated along the length of the plug can be theoretically integrated over the varying stress field. This relationship is mathematically represented by the following integral equation:

$$F_{plug} = \int_0^L \pi D_i(\sigma'_v(z) \cdot K_c \cdot tan\delta)dz + \sum_{j=1}^{N} \Delta u_j A_j$$

In this formula, the total plug resistance is calculated by integrating the product of the inner perimeter, the vertical effective stress, the lateral earth pressure coefficient, and the interface friction angle over the entire length of the soil plug [13]. The secondary summation term mathematically accounts for the residual dynamic uplift forces caused by localized transient pore-pressure gradients acting on discrete horizontal planes within the plug matrix. By continuously correlating the experimental values of plug resistance with the visual data provided by the pore-pressure imaging algorithm, the methodology establishes a direct, observable link between the microscopic hydraulic behavior and the macroscopic mechanical response of the caisson foundation [14]. This analytical framework forms the basis for all subsequent data interpretation and results analysis.

4. Results and Data Interpretation

4.1 Penetration Resistance and Plug Length Evolution

The physical modeling experiments yielded an exceptionally detailed continuous record of the mechanical response of the caisson during the entire penetration event. The total applied penetration force, which serves as a proxy for total penetration resistance, exhibited a distinct, highly non-linear progression that directly correlated with the physical evolution of the soil plug. During the initial phase of penetration, from the soil surface down to a normalized depth ratio of approximately two caisson diameters, the resistance increased linearly and relatively slowly. In this shallow regime, the laser displacement sensor confirmed that the soil was flowing freely into the inner cavity, maintaining an Incremental Filling Ratio of nearly 1.0. This indicated a classic fully coring mode, where the caisson wall simply sliced through the sand bed without inducing significant internal compaction. The total resistance measured during this phase was almost entirely attributable to the external shaft friction and the annular end-bearing capacity of the thin aluminum wall, while internal resistance remained negligible due to the short length of the developing soil column [15]. The lack of internal resistance permitted smooth, continuous penetration with minimal energy input, perfectly validating the theoretical advantages of open-ended caisson installation in shallow

profiles.

As the penetration depth progressed beyond three caisson diameters, a profound shift in the mechanical behavior was observed. The Incremental Filling Ratio began to deviate from unity, gradually decreasing to values between 0.6 and 0.8. This deviation marked the onset of the partially plugged state, where the internal soil column no longer advanced at the same rate as the external soil surface. The friction acting on the inner wall had accumulated to a point where it began to drag the outer perimeter of the soil plug downward, inducing severe shear strains and volumetric compaction within the core. Concurrently, the total penetration resistance began to rise at an exponential rate. The data revealed that the transition from coring to partial plugging is not an instantaneous event but rather a progressive mobilization of internal stresses [16]. As the plug lengthened, the structural phenomenon of soil arching began to take effect. The downward drag forces along the inner wall redirected the vertical stresses radially inward, creating a dense, self-supporting arch near the lower third of the plug. This localized densification dramatically increased the lateral earth pressures against the caisson wall, creating a positive feedback loop that rapidly amplified the internal friction. The critical experimental metrics capturing this transition across different penetration depths are documented in Table 3.

Table 3Plug Length and Penetration Resistance Correlation

Penetration Depth Ratio	Filling Mode Status	Incremental Filling Ratio	Total Resistance Force
1.0 Diameters	Fully Coring	0.98	4.2 Kilonewtons
3.0 Diameters	Transitional	0.85	11.5 Kilonewtons
5.0 Diameters	Partially Plugged	0.42	28.7 Kilonewtons
6.5 Diameters	Fully Plugged	0.05	54.3 Kilonewtons

The final stage of the penetration process was characterized by complete plug locking. At a normalized depth ratio of approximately 6.5 diameters, the Incremental Filling Ratio abruptly dropped to near zero, indicating that no further soil was entering the caisson. The soil plug had become fully locked, effectively transforming the open-ended caisson into a closed-ended pile. The macroscopic result was a massive, near-instantaneous spike in total penetration resistance, reaching a peak force that approached the operational limits of the servo-hydraulic actuator. The locked plug now acted as a rigid extension of the caisson itself, forcing all subsequent penetration to rely entirely on the deep bearing capacity of the soil beneath the plug toe. Upon post-test excavation, the soil plug was found to be highly overconsolidated and structurally intact, requiring significant mechanical effort to remove from the aluminum cavity. The physical measurements confirmed that the final Plug Length Ratio was significantly lower than unity, perfectly aligning with the dynamic displacement data recorded by the overhead laser sensor. This comprehensive mechanical dataset provided the necessary macroscopic context for interpreting the simultaneously recorded microscopic pore-pressure fields.

4.2 Spatiotemporal Pore-Pressure Distributions

The most significant contribution of this research is the successful generation and interpretation of the transient pore-pressure images. The implementation of the dynamic spatial interpolation algorithm transformed the complex web of sensor data into intuitive, high-resolution color-coded contour maps that visually depict the fluid pressure fields in real-time. During the initial fully coring phase, the images revealed a relatively symmetrical distribution of positive excess pore pressures concentrated immediately beneath the advancing annular tip of the caisson. The pressure gradients extended uniformly outward into the external soil mass and inward into the developing plug, dissipating rapidly as the fluid migrated away from the shear zone. The internal pore pressures within the upper portion of the plug remained essentially

hydrostatic, confirming that the soil was entering the cavity without significant radial compression or vertical confinement [17]. The lack of complex pressure gradients in the upper plug explained the absence of internal shaft friction during the fully coring stage, as the effective stresses remained low and unmodified by transient hydraulic forces.

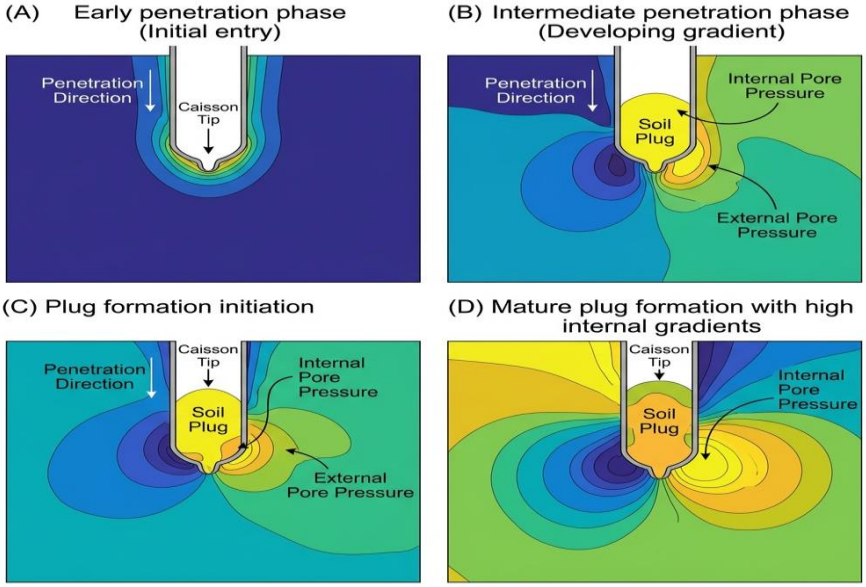


Figure 2: Spatiotemporal Transient Pore

As the penetration transitioned into the partially plugged regime, the pore-pressure images underwent a dramatic transformation. The internal pressure field became highly asymmetrical and stratified. A distinct zone of intense negative excess pore pressure, indicative of severe volumetric dilation, appeared adjacent to the inner caisson wall along the lower third of the plug. This visual observation provided direct physical evidence of the localized shear band formation theorized by discrete element models. The strong negative pore pressures in this shear zone temporarily increased the localized effective stress, acting as a hydraulic catalyst for the onset of soil arching. Concurrently, a zone of elevated positive excess pore pressure became trapped in the central core of the plug, bounded laterally by the dense shear bands and vertically by the impermeable mass of the compacted soil above [18]. This trapped fluid pressure significantly retarded the consolidation of the inner core, prolonging the transitional partially plugged state. The visual contrast between the dilating boundaries and the contracting core provided unprecedented insight into the complex micromechanics that govern the non-linear growth of plug resistance. The exact moment of full plug locking was distinctly captured by a sudden, systemic collapse of the internal hydraulic gradients. As the soil arch became fully established and the plug locked against the walls, the massive end-bearing stresses at the pile toe were transferred entirely through the solid soil skeleton. The pore-pressure images showed a rapid migration of intense positive excess pressures from the annular tip inward, coalescing into a massive pressure bulb directly beneath the locked plug toe. Inside the plug cavity, the dynamic pressure gradients instantly equalized, signaling the cessation of internal relative soil movement. The trapped fluid within the core began a slow, one-dimensional vertical dissipation process, decoupled from the external dynamic stresses. By overlaying the mechanical resistance data onto the sequential pore-pressure images, it became unequivocally clear that the sudden spike in penetration resistance was perfectly synchronized with the formation of the sub-toe pressure bulb. These visual correlations conclusively prove that monitoring internal pore-pressure gradients offers a highly sensitive, predictive method for anticipating plug locking before the catastrophic spike in ultimate resistance occurs, offering profound implications for real-time installation control.

5. Conclusion and Implications

5.1 Summary of Key Findings

This comprehensive experimental study has successfully demonstrated the viability and significant scientific value of utilizing transient pore-pressure imaging to investigate the complex mechanics of soil plugging during open-ended caisson penetration. By developing a highly sophisticated physical modeling apparatus equipped with an extensive array of miniature embedded sensors and utilizing dynamic spatial interpolation algorithms, the research transitioned geotechnical observation from discrete point measurements to continuous, full-field visualization. The macroscopic mechanical data thoroughly documented the classic transition from a low-resistance fully coring state to a high-resistance fully plugged state, characterized by the exponential growth of internal friction and a sudden drop in the Incremental Filling Ratio. More importantly, the concurrent microscopic fluid pressure data revealed the hidden hydromechanical drivers behind these macroscopic phenomena. The study empirically confirmed that plug formation is not merely a static frictional process, but a highly dynamic event heavily influenced by localized volumetric dilation, trapped fluid boundaries, and complex spatial pressure gradients.

The transient images explicitly captured the formation of distinct shear bands along the inner caisson wall, visually manifested as localized zones of negative excess pore pressure. These dilative zones were shown to temporarily spike the local effective stress, providing the necessary frictional resistance to initiate soil arching across the plug diameter. Furthermore, the visual data isolated the precise moment of plug locking, characterized by the sudden equalization of internal pressure gradients and the immediate formation of a massive positive pressure bulb beneath the plug toe [19]. This fundamental correlation between the collapse of internal fluid gradients and the instantaneous spike in total penetration resistance proves that transient pore-water dynamics are the primary governing precursors to mechanical plug failure. The ability to image these processes in real-time represents a major technological leap in laboratory soil-structure interaction studies, providing the highly resolute, continuous datasets required to validate and refine the next generation of advanced numerical modeling techniques.

5.2 Engineering Recommendations

The insights gained from this research have profound practical implications for the design and installation of offshore foundation systems. Current industry standards, which heavily rely on static, effective-stress-based empirical formulas, frequently underestimate the suddenness and severity of penetration refusal caused by unexpected plug locking in stratified or partially drained profiles. By recognizing that plug formation is governed by transient fluid dynamics, engineers can develop more accurate predictive models that incorporate the rate of penetration and the specific hydraulic conductivity of the site soils. For example, dynamically altering the penetration rate during installation could theoretically manage the dissipation of internal pore pressures, intentionally delaying the onset of soil arching and extending the fully coring depth [20]. If the installation equipment is equipped with internal pressure sensors, the real-time monitoring of pressure gradients could serve as an early warning system, allowing operators to adjust driving energy or utilize internal jetting before the plug becomes irreparably locked. Ultimately, integrating transient hydromechanical principles into standard geotechnical practice will lead to safer, more efficient, and significantly more cost-effective installation strategies for the massive open-ended caissons required by the expanding offshore energy sector.

References

Zhang, J., Peng, H., Sun, L., Wu, G., Liu, C., & Yu, Z. (2025, August). Unsupervised graph clustering with deep structural entropy. In Proceedings of the 31st ACM SIGKDD Conference on Knowledge Discovery and Data Mining V. 2 (pp. 3752-3763).

Ouyang, Z., & Mayne, P. W. (2021). Variable rate piezocone data evaluated using NTH limit plasticity solution. Geotechnical Testing Journal, 44(1), 174-190.

Ouyang, Z., Mayne, P. W., & Sharp, J. (2016). Review of clay chamber tests using miniature cone and piezocone penetrometers. Proceedings, GeoVancouver.

Ansari, A., Mandhaniya, P., Malik, B. A., & Ouyang, Z. (2025). Disaster risk and resilience assessment of multi-utility transportation infrastructure and urban projects. Frontiers in Built Environment, 11, 1619407.

Li, Y. Z., Zhang, J. P., Chen, Z. Y., Wang, H. C., Zhang, K. X., Hu, S. S., ... & Dudley, M. (2026, September). Growth and Characterization of High-Quality Thick Epitaxial 4H-SiC Wafers for High Voltage Devices. In Defect and Diffusion Forum (Vol. 452, pp. 79-85). Trans Tech Publications Ltd.

Li, X., Wang, P., Li, G., & Zhang, Y. (2023). Design of a novel self-test-on-chip interface ASIC for capacitive accelerometers. IEEE Transactions on Circuits and Systems I: Regular Papers, 70(7), 2834-2843.

Yu, A., Pang, F., Yuan, Y., Huang, Y., Li, S., Yu, S., ... & Xia, L. (2023). Simultaneous current and vibration measurement based on interferometric fiber optic sensor. Optics & Laser Technology, 161, 109223.

Yu, A., Huang, Y., Li, S., Wang, Z., & Xia, L. (2023). All fiber optic current sensor based on phase-shift fiber loop ringdown structure. Optics Letters, 48(11), 2925-2928.

Zhang, S., Huang, P., & Yan, W. (2024). A data-driven approach for railway in-train forces monitoring. Advanced Engineering Informatics, 59, 102258.

Lu, J., Xiong, H., Zhou, J., Lin, Z., & Feng, B. (2025, September). Collaborative Spatial and Channel Attention for Structural Vibration-based Gait Recognition. In 2025 IEEE International Joint Conference on Biometrics (IJCB) (pp. 1-11). IEEE.

Zhao, R., Tang, J., Zeng, W., Guo, Y., & Zhao, X. (2025). Towards human-like questioning: Knowledge base question generation with bias-corrected reinforcement learning from human feedback. Information Processing & Management, 62(3), 104044.

Zhao, R., Tang, J., Zeng, W., Chen, Z., & Zhao, X. (2024, October). Zero-shot knowledge graph question generation via multi-agent llms and small models synthesis. In Proceedings of the 33rd ACM International Conference on Information and Knowledge Management (pp. 3341-3351).

Li, Q., Ye, Q., Zhang, N., Zhang, W., & Hu, F. (2025). Digital-twin-enabled industrial IoT: Vision, framework, and future directions. IEEE Wireless Communications, 32(6), 173-181.

Li, S. (2025). Momentum, volume and investor sentiment study for us technology sector stocks—A hidden markov model based principal component analysis. PloS one, 20(9), e0331658.

Zhang, B., Wang, S., Jiang, Y., Sui, D., Tu, Z., & Chu, D. (2025, July). Ask and Retrieve Knowledge: Towards Proactive Asking with Imperfect Information in Medical Multi-turn Dialogues. In Proceedings of the 48th International ACM SIGIR Conference on Research and Development in Information Retrieval (pp. 1055-1065).

Hu, H., Yang, Y., Zhao, Q., & Zhang, C. (2022, June). On the role of discount factor in offline reinforcement learning. In International conference on machine learning (pp. 9072-9098). PMLR.

Wang, Z., Yuan, R., Geng, Z., Li, H., Qu, X., Li, X., ... & Zhang, K. (2025, October). Singing timbre popularity assessment based on multimodal large foundation model. In Proceedings of the 33rd ACM International Conference on Multimedia (pp. 12227-12236).

Peng, Y., Li, H., BouDagher-Fadel, M., Wang, L., Zhang, D., Zheng, T., & Yang, K. (2022). Benthic foraminifera distribution and sedimentary environmental evolution of a carbonate platform: A case study of the Guadalupian (middle Permian) in eastern Sichuan Basin. Marine Micropaleontology, 170, 102079.

Lyu, M., Torii, R., Liang, C., Li, Q., Wang, X., Ventikos, Y., & Chen, D. (2025). In silico comparison of two non-invasive pre-procedural virtual coronary revascularisation techniques for personalised cardiovascular medicine. Computer Methods and Programs in Biomedicine, 109046.

Emani, M., Xie, Z., Raskar, S., Sastry, V., Arnold, W., Wilson, B., ... & Boyd, M. (2022, November). A comprehensive evaluation of novel AI accelerators for deep learning workloads. In 2022

IEEE/ACM international workshop on performance modeling, benchmarking and simulation of high performance computer systems (PMBS) (pp. 13-25). IEEE.